way of generating atomically well-defined edges that make graphene-based electronics possible.

References and Notes

1. K. S. Novoselov *et al.*, *Science* **306**, 666 (2004).
2. K. S. Novoselov *et al.*, *Proc. Natl. Acad. Sci. U.S.A.* **102**, 10451 (2005).
3. Y. Zhang, Y. W. Tan, H. L. Stormer, P. Kim, *Nature* **438**, 201 (2005).
4. J. C. Meyer *et al.*, *Nature* **446**, 60 (2007).
5. A. K. Geim, K. S. Novoselov, *Nat. Mater.* **6**, 183 (2007).
6. Y. W. Son, M. L. Cohen, S. G. Louie, *Nature* **444**, 347 (2006).
7. X. Li, X. Wang, L. Zhang, S. Lee, H. Dai, *Science* **319**, 1229 (2008); published online 23 January 2008 (10.1126/science.1150878).
8. T. Enoki, Y. Kobayashi, K. Fukui, *Int. Rev. Phys. Chem.* **26**, 609 (2007).
9. K. Nakada, M. Fujita, G. Dresselhaus, M. S. Dresselhaus, *Phys. Rev. B* **54**, 17954 (1996).
10. K. Wakabayashi, *Phys. Rev. B* **64**, 125428 (2001).
11. L. G. Cançado *et al.*, *Phys. Rev. Lett.* **93**, 047403 (2004).
12. L. G. Cançado, M. A. Pimenta, B. R. A. Neves, M. S. S. Dantas, A. Jorio, *Phys. Rev. Lett.* **93**, 247401 (2004).
13. P. Shemella, Y. Zhang, M. Mailman, P. M. Ajayan, S. K. Nayak, *Appl. Phys. Lett.* **91**, 042101 (2007).
14. L. Yang, C. H. Park, Y. W. Son, M. L. Cohen, S. G. Louie, *Phys. Rev. Lett.* **99**, 186801 (2007).
15. X. Wang *et al.*, *Phys. Rev. Lett.* **100**, 206803 (2008).
16. T. C. Li, S. P. Lu, *Phys. Rev. B* **77**, 085408 (2008).
17. F. Cervantes-Sodi, G. Csányi, S. Piscanec, A. C. Ferrari, *Phys. Rev. B* **77**, 165427 (2008).
18. L. Tapasztó, G. Dobrik, P. Lambin, L. P. Biró, *Nat. Nanotechnol.* **3**, 397 (2008).
19. M. Y. Han, B. Özyilmaz, Y. Zhang, P. Kim, *Phys. Rev. Lett.* **98**, 206805 (2007).
20. J. Campos-Delgado *et al.*, *Nano Lett.* **8**, 2773 (2008).
21. F. Banhart, *Rep. Prog. Phys.* **62**, 1181 (1999).
22. B. T. Kelly, *Physics of Graphite* (Applied Science Publishers, London, 1981).
23. J. Goma, A. Oberlin, *Thin Solid Films* **65**, 221 (1980).
24. J. N. Rouzaud, A. Oberlin, C. Beny-Bassez, *Thin Solid Films* **105**, 75 (1983).
25. C. Jin, K. Suenaga, S. Iijima, *Nano Lett.* **8**, 1127 (2008).
26. Y. W. Son, M. L. Cohen, S. G. Louie, *Phys. Rev. Lett.* **97**, 216803 (2006).
27. M. Vandescuren, P. Hermet, V. Meunier, L. Henrard, Ph. Lambin, *Phys. Rev. B* **78**, 195401 (2008).
28. S. Latil, V. Meunier, L. Henrard, *Phys. Rev. B* **76**, 201402 (2007).
29. D. A. Areshkin, D. Gunlycke, C. T. White, *Nano Lett.* **7**, 204 (2007).
30. We thank Z. Ren, S. Chen, B. I. Yakobson, S. Gradecak, G. Dresselhaus, and G. Chen for valuable and fruitful discussions, and E. Gracia-Espino for providing the Pt-coated ribbons that we used in some experiments.

This work was supported by NSF grant Nanoscale Interdisciplinary Research Teams CTS-05-06830. We also thank Consejo Nacional de Ciencia y Tecnología (CONACYT)–Mexico for grants 56787 (Laboratory for Nanoscience and Nanotechnology Research–LINAN), 45772 (M.T.), 41464–Interamerican Collaboration (M.T.), 2004-01-013/SALUD-CONACYT (M.T.), and Ph.D. scholarships (J.C.-D. and J.M.R.-H.). A portion of the present research was supported in part by the Laboratory Directed Research and Development Program of ORNL, managed by UT-Battelle, by the Division of Materials Science and Engineering, U.S. Department of Energy, and by the Center for Nanophase Materials Sciences, sponsored by the Division of Scientific User Facilities, U.S. Department of Energy (V.M. and B.G.S.). A patent that is related to the production of these graphic nanoribbons has been submitted by some of the authors and holds the U.S. patent application number 12/042,544.

Supporting Online Material

www.sciencemag.org/cgi/content/full/323/5922/1701/DC1
Materials and Methods
SOM Text
Figs. S1 to S6
References

6 October 2008; accepted 10 February 2009
10.1126/science.1166862

Graphene at the Edge: Stability and Dynamics

Çağlar Ö. Girit,[1,2] Jannik C. Meyer,[1,2] Rolf Erni,[3] Marta D. Rossell,[3] C. Kisielowski,[3] Li Yang,[1,2] Cheol-Hwan Park,[1,2] M. F. Crommie,[1,2] Marvin L. Cohen,[1,2] Steven G. Louie,[1,2] A. Zettl[1,2]*

Although the physics of materials at surfaces and edges has been extensively studied, the movement of individual atoms at an isolated edge has not been directly observed in real time. With a transmission electron aberration–corrected microscope capable of simultaneous atomic spatial resolution and 1-second temporal resolution, we produced movies of the dynamics of carbon atoms at the edge of a hole in a suspended, single atomic layer of graphene. The rearrangement of bonds and beam-induced ejection of carbon atoms are recorded as the hole grows. We investigated the mechanism of edge reconstruction and demonstrated the stability of the "zigzag" edge configuration. This study of an ideal low-dimensional interface, a hole in graphene, exhibits the complex behavior of atoms at a boundary.

Graphene, a single atomic layer of carbon atoms bonded in a hexagonal lattice, is one of few materials that are stable in two dimensions (*1*) and free-standing when suspended (*2*). This unexpected stability (*3*), combined with its exotic band structure and other unusual physical properties (*4*), has led to a considerable amount of experimental research (*5*–*11*). Of the many theoretical studies of graphene, a substantial portion are devoted to the physics of graphene edges, whose structure in narrow graphene ribbons is predicted to have a major impact on their electronic properties (*12*, *13*). Experimental studies of the graphene edge have lagged behind, mainly due to the difficulty of atomically resolving and characterizing the boundaries of graphene sheets, but would give insight into the one-dimensional (1D) interface of a purely 2D structure.

The traditional method of obtaining atomic resolution on surfaces and edges is scanning tunneling microscopy (STM) or atomic force microscopy (AFM). Although there are several atomically resolved AFM/STM studies of graphene (*14*–*16*), as well as studies of step edges in graphite (*17*), there are several problems in observing dynamics of the edge atoms with scanning probe techniques. First, typical scan speeds are on the order of minutes to hours, which may be too slow to capture the movement of atoms. Second, the highest resolution and stability is obtained at cryogenic temperature, where the dynamics may be frozen out. Finally, the sample is usually on a substrate, which can strongly influence the behavior of atoms both in the bulk and at the edge. To observe dynamics on a time scale of seconds, the only alternative to scanning probe microscopes with comparable spatial resolution is the transmission electron microscope (TEM). Indeed, the dynamics of atom columns composed of heavy atoms were observed in this manner (*18*).

Traditional TEMs lack the necessary resolution at the low operating voltages required to avoid immediate sample damage. Previous 100 to 200 kV TEM studies of few-layer graphitic materials showed that some microscopes have difficulty resolving the lattice and are not capable of atomically resolving edges (*19*–*21*), making image interpretation ambiguous. By using the Transmission Electron Aberration-corrected Microscope monochromated (TEAM 0.5) (*22*), capable of sub-Ångstrom resolution even at 80 kV, we imaged every carbon atom in the lattice of suspended single-layer graphene (*23*). We employed the same microscope to record the dynamics of carbon atoms on the edge of a hole in a graphene sheet. The sample was prepared as described previously (*24*), and details of the microscope configuration can be found in (*23*). The entire experiment was conducted in the high-vacuum environment ($<10^{-7}$ mbar) of the microscope chamber.

Movie S1 shows the evolution of the hole within a suspended graphene sheet. Each frame averages 1 s of exposure, and the frames themselves are 4 s apart. The carbon atoms are shown as white because the spherical aberration was chosen to be negative (*25*). The spatial sampling is 26 ± 4 pm/pixel, determined by fitting for the measured atomic positions and using the known atomic spacing of 1.42 Å. Figure 1A shows the first frame of the sequence. The hole, initially formed through prolonged irradiation by the electron beam, is clearly visible near the center of the frame and is surrounded by the hexagonal carbon lattice. The structures lining the boundary of the frame are adsorbates

[1]Department of Physics, University of California at Berkeley, Berkeley, CA 94720, USA. [2]Materials Sciences Division, Lawrence Berkeley National Laboratory, Berkeley, CA 94720, USA. [3]National Center for Electron Microscopy, Lawrence Berkeley National Laboratory, Berkeley, CA 94720, USA.

*To whom correspondence should be addressed. E-mail: azettl@berkeley.edu

most likely deposited during the process of suspending the graphene sheet. Every carbon atom in the lattice is resolved, including those at the edge of the hole. Although there is a possibility that edge atoms could be terminated by hydrogen or other functional groups, there is no reason experimentally to indicate that this is the case, and the results of simulation show that this would not have an effect on the observed dynamics (*26*). As the sheet is suspended, small drifts in the *z* direction can occasionally move it out of the focal plane of the microscope. To account for this, a focal adjustment was made between frames 29 and 30, which represents a time gap of less than 1 minute.

Figure 1, B and C, showing frames 9 and 10 of movie S1, respectively, depict the basic mechanism by which the hole changes shape. While motion of the atoms is expected to occur faster than the 1-s sampling time in the experiment, it is the "meta-stable" configurations of the edge that are recorded. The dashed line in Fig. 1, B and C, circles a hexagon which "loses" two atoms, indicated by red diamonds, as a result of either knock-on damage from the electrons in the beam or migration to vacant sites nearby. For an 80-keV incident electron, the maximum energy that can be transferred to a carbon atom is 15.8 eV (*27*). The knock-on energy threshold for ejection of an in-lattice carbon atom with three bonds is 17 eV, corresponding to a beam energy of 86 keV (*28*), and hence those atoms are not ejected. However, this threshold drops below the maximum transfer energy to 15 eV for sites with a neighboring vacancy (*29*) and may be even less in our case, where atoms at the edge may have several vacant next-nearest-neighbor sites. The lower energy mechanism of beam-induced ejection of atoms from the edge, as opposed to the surface, is referred to as sputtering and is responsible for the overall enlargement of the hole.

The energy barrier for migration of a carbon atom to various nearby vacant sites is expected to be less than the 15 eV necessary for sputtering. Indeed, ab initio density functional theory (DFT) calculations within the local density approximation give a barrier height of 0.3 to 6.6 eV for unterminated edges (*26*). Because of the much smaller energy threshold for atom migration, these events should occur more frequently than hole enlargement, and this is what is observed. Movie S1 and subsequent figures show that the hole growth time scale is on the order of minutes, in contrast to less than a second for edge reconfiguration. Figure 1, B and C, shows the appearance of two carbon atoms (blue dots) at previously vacant sites. This may be a result of migration of the two atoms indicated by red diamonds or from another region of the hole. It is also possible that the region of the hole obscured by adsorbates acts as a carbon atom reservoir, which can replenish sites that are made vacant. Those adsorbates are likely rich in carbon and more reactive than graphene, providing atoms for "repair" of the lattice but at a slower rate than beam-induced ejection, leading to an overall growth of the hole. These competing mechanisms result in the rich dynamics observed in the movie.

To investigate whether a model can reproduce the experimental observations, we simulate the evolution of the graphene hole with a kinetic Monte Carlo method (*26*, *30*). We manually define a hole in a graphene lattice and describe the edge dynamics in terms of three different mechanisms: the beam-induced ejection of carbon atoms along the edge, the addition of carbon atoms from a virtual reservoir, and the migration of dangling carbon atoms from one site to another. The ejection probability incorporates the effect of energy input from the electron beam. The addition probability, smaller than the ejection probability, accounts for the possibility of obtaining carbon atoms from either the imperfect vacuum in the microscope or adsorbates near the hole. These two probabilities are estimated to be much smaller than the migration probabilities and thus set by hand. The migration probabilities (up to the third nearest-neighbor sites) are determined by the factor $e^{-\frac{\Delta E}{k_B T}}$, where ΔE is the relevant energy barrier height obtained from DFT calculations and T is an effective temperature corresponding to the energy input from the electron beam. In the movie of simulated hole growth (movie S2), the time step is not necessarily that of the experimental movie (movie S1). The dynamics, as characterized by Figs. 2 and 3, are remarkably similar to that observed experimentally and show the emergence of long-range order and the mechanism of edge reconfiguration.

Figure 2 shows typical examples from the experiment of edge configurations with a high degree of order. The outlined region of the hole in Fig. 2A is entirely "armchair," and that in Fig. 2B

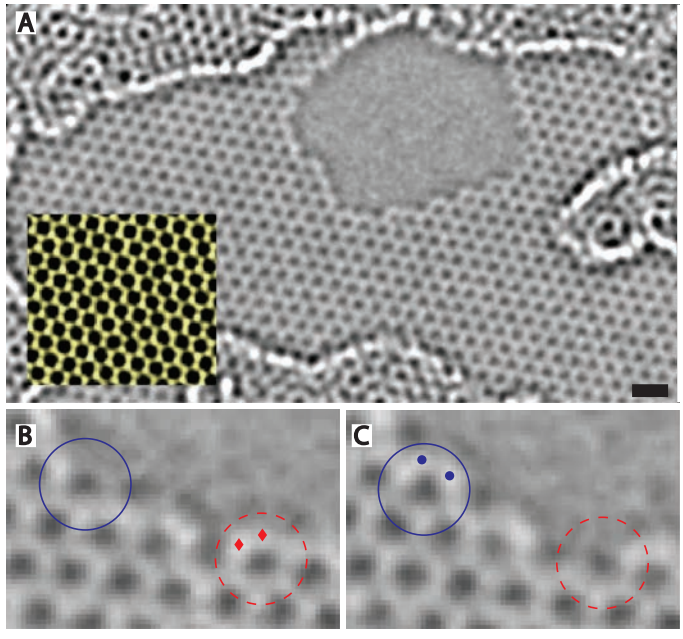

Fig. 1. (**A**) Aberration-corrected TEM image of a hole in a single layer of graphene produced by prolonged irradiation (frame 1 of Movie S1). Individual carbon atoms are resolved as white spots. Structures lining the perimeter are adsorbates. Scale bar is 5 Å. (Inset) Averaged series of images showing the atomically resolved graphene lattice. (**B**) and (**C**) Two still frames (9 and 10) in the evolution of the hole, with (C) following 4 s after (B). Two carbon atoms (red diamonds in the dashed circle) are removed while two carbon atoms nearby (blue dots) bind to their neighbors to close a hexagon (solid circle). The measured lattice constant is 2.5 Å ± 0.2 Å.

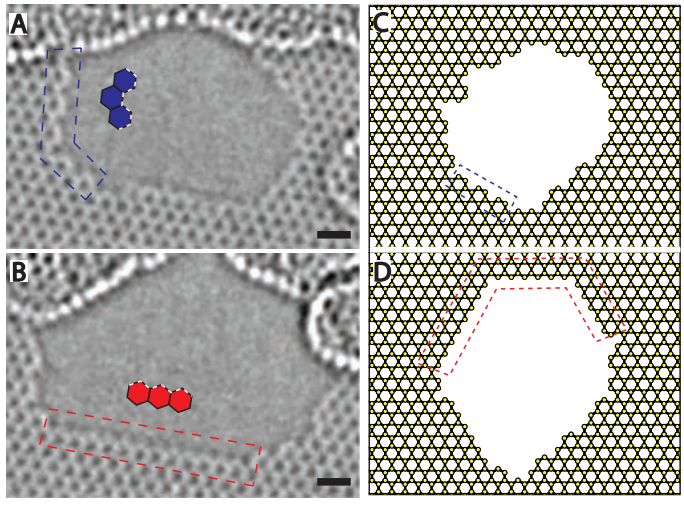

Fig. 2. Edge configurations. Aberration-corrected TEM image of (**A**) an armchair (frame 24) and (**B**) zigzag (frame 55) configuration of carbon atoms at the edge of a hole in graphene. The inset diagrams exemplify an armchair (upper panel) and zigzag (lower panel) arrangement. The armchair edge, roughly 12 hexagons long, makes a 60° turn at the lower left-hand corner. The zigzag edge is a continuous segment 12 hexagons long. Examples of the emergence of long-range order in the simulation of hole growth are (**C**), frame 113, with a 7-hexagon armchair segment at the edge of the simulated hole and (**D**), frame 223, an extremely long (19 hexagon) zigzag edge interrupted by two 60° turns.

is entirely "zigzag." These two configurations are defined in the inset diagrams of Fig. 2, A and B, respectively. Each ordered edge spans about 12 hexagons. The existence of such long-range order indicates that these configurations are stable, at least for periods of time longer than the 1 s to capture the frame. Such long-range order is also observed in the simulation, as shown in Fig. 2, C and D, where a 7-hexagon armchair edge and a 19-hexagon zigzag edge are identified, respectively. Long armchair edges are much less prevalent than zigzag edges in the simulation. This is also the case experimentally, although not as pronounced, and results from the greater stability of the zigzag edge.

The beam-induced ejection of atoms, and the resultant migration and edge reconfiguration, changes the shape of the hole, as shown in Fig. 3A. An armchair sequence at a corner of the hole transforms over the course of 4 s, or one frame, into a zigzag sequence. The blue dots in the upper frame indicate two carbon atoms that were removed from the armchair edge, and the red diamonds in the lower frame indicate four atoms added to form the zigzag edge. At a corner, or for a short segment, such a transformation would only involve the migration, addition, or removal of a handful of atoms, but the exact sequence of events is unknown. For long, uniform segments such as in Fig. 2, B or D, where the edge is aligned with the zigzag direction of the lattice, a transformation to armchair is difficult. Similar behavior is again observed in the simulation, where the rearrangement of atoms can also interconvert armchair and zigzag edges. The simplest example of such an event is shown in Fig. 3B, where three atoms on a zigzag edge (red diamonds, upper frame) disappear and within four frames, two others appear (blue dots, lower frame) to form an armchair edge.

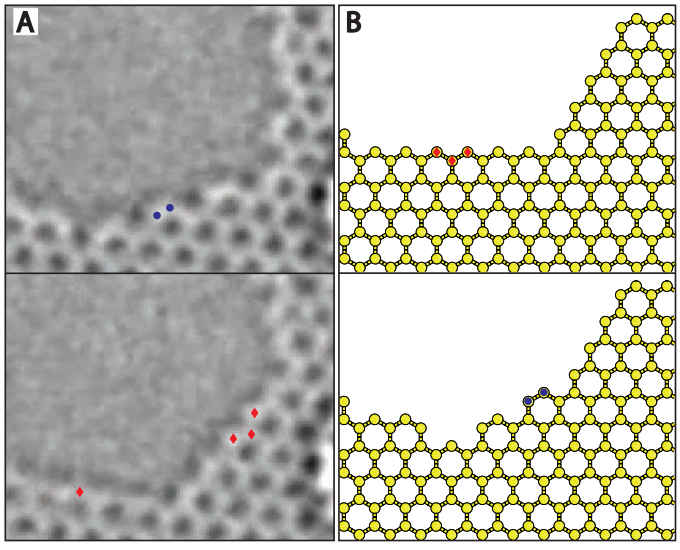

Fig. 3. Edge reconfiguration. (**A**) Conversion of an armchair edge (top) to a zigzag edge (bottom) over the course of two frames, 14 and 15, taken at a 4-s interval. The two atoms marked as blue dots in the upper frame are gone in the lower frame, where four new carbon atoms are indicated as red diamonds. The 7- hexagon armchair edge is transformed into a 9-hexagon zigzag edge with a 60° turn. The transformation occurs due to migration of atoms along the edge. (**B**) Similar behavior is observed in the kinetic Monte Carlo simulation of hole growth, where three zigzag atoms (red diamonds, top) from frame 235 disappear and two armchair atoms (blue dots, bottom) appear in frame 239. Both frames in (B) have been flipped vertically.

In Fig. 4, we analyze the data in an attempt to understand the growth of the hole as a function of time and demonstrate the stability of the zigzag edge configuration. Figure 4A shows a flattened image averaging all 110 recorded frames. First, the images are registered by taking the initial frame, isolating a region of the lattice far from the hole, and shifting all subsequent frames into alignment (*30*). Then the pixel values are averaged over all frames to produce an image. The advantage of such a representation is that it will highlight structures along the edge that appear often, even though those structures may change rapidly from frame to frame. Faint hexagons are fleeting, located in regions where the hole quickly grew in size, whereas well-contrasted hexagons are more stable and existed throughout most of the recording. One observes that the most prominent edge structure is of the zigzag type, with the bottom and lateral sides of the hole aligned in the zigzag directions of the lattice. The faint hexagons are concentrated on the left and right sides of the hole, where the hole grew quickly. The dashed line indicates a path of pixels along which the time development is shown in Fig. 4B. The pixel values along the path are lined on the horizontal axis, with the vertical axis time going from top to bottom. The hexagons are indicated by alternating bands of black and white, with the hole a uniform gray. Here, one directly sees the growth of the hole along the cut in Fig. 4A. The hole expands by roughly three hexagons both to the left and the right within the first 50 frames and then stabilizes with about two hexagons on the left side and one on the right. This stable configuration corresponds to the formation of zigzag edges on the left and right of Fig. 4A. The lateral regions of the hole, which started with more armchair or mixed-type edges, stabilize in a state that is more zigzag in nature. A similar slice taken perpendicular to the bottom edge of the hole (not shown) indicates a slower growth of the hole in that direction, indicating that it is difficult to erode the long zigzag edge. To further analyze the hole growth, the outline of the hole was determined algorithmically for each frame. All such outlines were averaged over all frames to produce the image in Fig. 4C. Faint lines indicate regions where the outline quickly

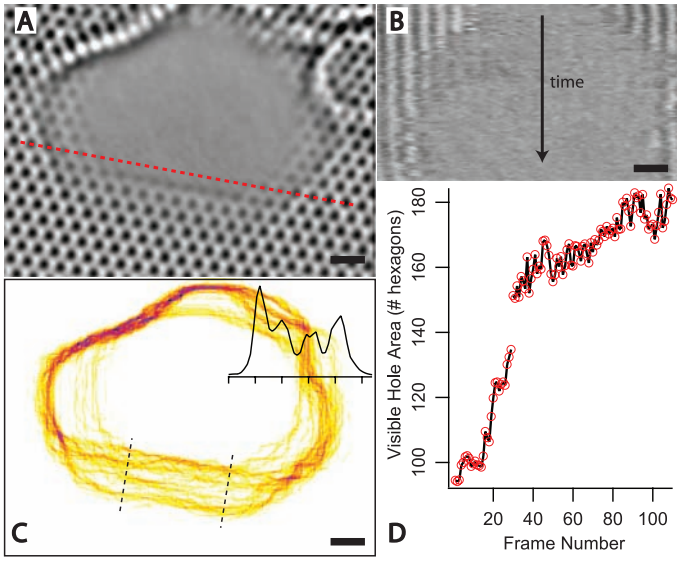

Fig. 4. Growth of hole in graphene. (**A**) Average intensity map constructed by averaging pixel values over all 110 frames of movie S1 after frame registration. Faint hexagons in the interior have been gradually removed by knock-on damage from the electron beam. Scale bar is 5 Å. (**B**) Time development of the pixel values along the dashed line in (A). The left end of the dashed line corresponds to the left side of (B). The frame number increases from top to bottom, and the scale bar is 5 Å along the *x* axis (position) and 30 frames, or 120 s, along the *y* axis (time). The opening of the hole is visible as a reduction in the number of black-and-white bands, corresponding to hexagons, scanning downwards. (**C**) Average, over all frames, of the perimeter of the hole. Darker segments of lines correspond to regions through which the perimeter passed more often than lighter segments. The hole opened quickly in the horizontal direction, as observed in (B), but near the bottom edge, the presence of four dark bands indicates that those configurations of the perimeter were more stable and the hole opened less quickly in the direction of the black dashed line. Scale bar is 5 Å. (Inset) The profile of pixel values along the dashed line shows four peaks corresponding roughly to the graphene lattice constant. Tick spacing, 2 Å. (**D**) The visible area of the hole, normalized by the area of a single hexagon, 5.17 $Å^2$, as a function of frame number. The missing line segment indicates the 30-s gap between frames 29 and 30.

changed shape and darker ones where the outline of the hole was more constant. The analysis of the lateral and bottom regions is similar to the above, except that one clearly sees four bands on the bottom (between dashed lines) aligned along the zigzag direction. This indicates once more that the hole was more stable along that direction and that the hexagons remained in place longer. An averaged line profile over those bands shows four peaks (inset, Fig. 4C), with a mean spacing of 2.1 Å, close to the lattice constant of 2.46 Å. Finally, in Fig. 4D, the area within the hole, as determined from the outlines, is computed and plotted as a function of frame number. We see the sharp increase in area within the first 50 frames as the hexagons along the left and right edges of the hole are removed, and then the hole growth slows down as a more stable configuration and a larger hole is produced. This global analysis of the edge stability is complemented by a site-by-site analysis of the zigzag fraction (fig. S1).

A simple model can account for the stability of zigzag edges observed in both experiment and simulation by considering the effect of ejecting an atom at the edge for each chirality (fig. S2). Half of the atoms along a zigzag or armchair edge are bonded to two neighboring atoms, and the other half are bonded to three neighboring atoms. Naively, we expect that the atoms most likely to be ejected by the electron beam are those with two neighboring atoms. The removal of such an atom from a zigzag edge leaves a vacancy without creating any dangling carbon atoms, those bonded to only a single neighbor. However the removal of such an atom from an armchair edge does leave a dangling carbon atom, which can easily migrate and fill a vacancy elsewhere on the edge, as the calculations predict (*30*). For an armchair configuration, two atoms are needed to repair the edge: the atom that was ejected and the neighboring dangling atom that migrated away. In a zigzag edge, only the ejected atom needs replacement. Hence, the zigzag edge is more stable under electron irradiation at this energy, and the argument holds even when the ejection of atoms along the edge with three neighbors is considered.

The images, simulation, and analysis presented here show the complicated dynamics that occur at the atomic edge of a single-layer graphene sheet. The TEAM microscope provides real-time atomic resolution, and the electron beam at 80 keV acts as an energy bath that allows the dynamics of edge reconstruction and hole growth to be observed. In our study of the edge configuration, we demonstrate the stability of the armchair and zigzag arrangements and quantify their evolution with time. Although the reconfiguration occurs on a time scale on the order of seconds, with a comparable contribution of armchair and zigzag sites, the long-term stability of zigzag edges is elucidated through a time-average analysis and explained by a simple model.

References and Notes

1. K. S. Novoselov *et al.*, *Science* **306**, 666 (2004).
2. J. C. Meyer *et al.*, *Nature* **446**, 60 (2007).
3. K. S. Novoselov *et al.*, *Proc. Natl. Acad. Sci. U.S.A.* **102**, 10451 (2005).
4. A. K. Geim, K. S. Novoselov, *Nat. Mater.* **6**, 183 (2007).
5. K. S. Novoselov *et al.*, *Nature* **438**, 197 (2005).
6. Y. Zhang, Y.-W. Tan, H. L. Stormer, P. Kim, *Nature* **438**, 201 (2005).
7. Y. Zhang *et al.*, *Nat. Phys.* **4**, 627 (2008).
8. S. Y. Zhou *et al.*, *Nat. Phys.* **2**, 595 (2006).
9. T. Ohta, A. Bostwick, T. Seyller, K. Horn, E. Rotenberg, *Science* **313**, 951 (2006).
10. J. S. Bunch *et al.*, *Science* **315**, 490 (2007).
11. C. Lee, X. Wei, J. W. Kysar, J. Hone, *Science* **321**, 385 (2008).
12. L. Yang, C.-H. Park, Y.-W. Son, M. L. Cohen, S. G. Louie, *Phys. Rev. Lett.* **99**, 186801 (2007).
13. Y.-W. Son, M. L. Cohen, S. G. Louie, *Nature* **444**, 347 (2006).
14. V. W. Brar *et al.*, *Appl. Phys. Lett.* **91**, 122102 (2007).
15. G. M. Rutter *et al.*, *Science* **317**, 219 (2007).
16. M. Ishigami, J. H. Chen, W. G. Cullen, M. S. Fuhrer, E. D. Williams, *Nano Lett.* **7**, 1643 (2007).
17. L. Tapaszto, G. Dobrik, P. Lambin, L. P. Biro, *Nat. Nano.* **3**, 397 (2008).
18. A. V. Martin, K. Ishizuka, C. Kisielowski, L. J. Allen, *Phys. Rev. B* **74**, 172102 (2006).
19. J. C. Meyer, C. O. Girit, M. F. Crommie, A. Zettl, *Nature* **454**, 319 (2008).
20. J. Campos-Delgado *et al.*, *Nano Lett.* **8**, 2773 (2008).
21. M. H. Gass *et al.*, *Nat. Nano.* **3**, 676 (2008).
22. C. Kisielowski *et al.*, *Microsc. Microanal.* **14**, 454 (2008).
23. J. C. Meyer *et al.*, *Nano Lett.* **8**, 3582 (2008).
24. J. C. Meyer, C. O. Girit, M. F. Crommie, A. Zettl, *Appl. Phys. Lett.* **92**, 123110 (2008).
25. K. W. Urban, *Science* **321**, 506 (2008).
26. Materials and methods are available as supporting material on *Science* Online.
27. R. F. Egerton, F. Wang, P. A. Crozier, *Microsc. Microanal.* **12**, 65 (2006).
28. B. W. Smith, D. E. Luzzi, *J. Appl. Phys.* **90**, 3509 (2001).
29. V. H. Crespi, N. G. Chopra, M. L. Cohen, A. Zettl, S. G. Louie, *Phys. Rev. B* **54**, 5927 (1996).
30. A. F. Voter, in *Proceedings of the NATO Advanced Study Institute on Radiation Effects in Solids* (Springer, Berlin, 2006), pp. 1–23.

31. The National Center for Electron Microscopy is supported by the Department of Energy under contract DE-AC02-05CH11231. The TEAM project is supported by the Department of Energy, Office of Science, Office of Basic Energy Sciences. Ç.G., J.M., and A.Z. were supported by the Director, Office of Energy Research, Office of Basic Energy Sciences, Materials Sciences, and Engineering Division, of the U.S. Department of Energy under contract DE-AC02-05CH11231, through the sp^2-bonded nanostructures program. L.Y., C.-H.P., M.L.C., and S.G.L. were supported by the National Science Foundation and by the Director, Office of Science, Office of Basic Energy Science, Division of Material Sciences and Engineering, U.S. Department of Energy. Ç.G. thanks P. Vollhardt, V. W. Brar, and Y. Zhang for interesting discussions.

Supporting Online Material

www.sciencemag.org/cgi/content/full/323/5922/1705/DC1
Materials and Methods
Figs. S1 and S2
References
Movies S1 and S2

9 October 2008; accepted 30 January 2009
10.1126/science.1166999

Reversible Interactions with para-Hydrogen Enhance NMR Sensitivity by Polarization Transfer

Ralph W. Adams,[1] Juan A. Aguilar,[1] Kevin D. Atkinson,[1] Michael J. Cowley,[1] Paul I. P. Elliott,[1]* Simon B. Duckett,[1]† Gary G. R. Green,[2] Iman G. Khazal,[1] Joaquín López-Serrano,[1] David C. Williamson[1]

The sensitivity of both nuclear magnetic resonance spectroscopy and magnetic resonance imaging is very low because the detected signal strength depends on the small population difference between spin states even in high magnetic fields. Hyperpolarization methods can be used to increase this difference and thereby enhance signal strength. This has been achieved previously by incorporating the molecular spin singlet para-hydrogen into hydrogenation reaction products. We show here that a metal complex can facilitate the reversible interaction of para-hydrogen with a suitable organic substrate such that up to an 800-fold increase in proton, carbon, and nitrogen signal strengths are seen for the substrate without its hydrogenation. These polarized signals can be selectively detected when combined with methods that suppress background signals.

The wide variety of applications of nuclear magnetic resonance (NMR) (*1*–*3*) are limited by the technique's extremely low inherent sensitivity. Here we describe an approach that uses hyperpolarized spins derived from para-hydrogen (para-H_2) (*4*) to sensitize the NMR experiment without actually incorporating para-H_2 into the molecule that is to be probed. Specifically, we show that high-resolution NMR spectra can be collected for a range of molecules and nuclei with detected signal strengths up to 800 times greater than would be normally achievable with an unpolarized sample. This improvement facilitates the collection of diagnostic high-resolution ^{1}H, ^{13}C, ^{15}N, and ^{19}F NMR spectra and magnetic resonance images of selected signals in a fraction of the time that would normally be necessary. When optimized, this route is predicted to increase proton sensitivity by up to four orders of magnitude (*5*) such that the routine single shot characterization of materials, even at picomole levels, will become possible (*6*).